SPECTROSCOPY STUDY OF CHARGE TRANSPORT IN ORGANIC FIELD-EFFECT TRANSISTORS

Lim Yong Hui

A0083136J

Supervisors:

Asst. Prof. CHUA Lay-Lay

Dr. GUO Han

A THESIS SUBMITTED IN PARTIAL FULFILMENT FOR THE DEGREE FOR

BACHELOR OF SCIENCE (HONOURS) IN PHYSICS

DEPARTMENT OF PHYSICS

NATIONAL UNIVERSITY OF SINGAPORE

ACADEMIC YEAR 2014/2015

ABSTRACT

Poly{[*N*,*N*'-bis(2-octyldodecyl)-naphthalene-1,4,5,8-bis(dicarboximide)-2,6-diyl]-alt-5,5'-(2,2'-bithiophene)}, or P(NDI2OD-T2), is one of the recently studied air-stable donor-acceptor n-type polymer with high electron mobility. In this project, top-gate bottom-contact field-effect transistor (FET) devices are fabricated to study the charge transport of P(NDI2OD-T2) as a function of different gate dielectric polymers using charge modulation spectroscopy (CMS) technique. Room temperature CMS data revealed a charge-induced absorption peak around 1.60 eV that indicated the dependence of the degree of charge carrier delocalization on gate dielectric, i.e. the degree of delocalization increased while the dielectric constant (k) decreased, in correlation with higher electron mobility and lower FET activation energy in lower k devices. Hence, while previous CMS studies of P(NDI2OD-T2) suggested significant localization of polarons in single polymer chain, this project reveals its delocalized nature in the semiconductor with need for further CMS characterization in the mid-infrared (MIR) region.

ACKNOWLEDGEMENTS

TABLE OF CONTENTS

1   INTRODUCTION

Carbon-based molecules and polymers semiconductors were first reported almost 50 years ago.[1] The research on their potential application in electronic devices such as light-emitting diodes, field-effect transistors, and photovoltatics started in the late 1980s, and ever since, great effort from both the electronic industry and the academia has led to rapid progress in the field of organic electronics.[2,3,4]

The organic field-effect transistors (OFETs) based on conjugated polymers offeres several advantages over traditional silicon transistors. Owing to the good solution-processability of conjugated polymers, the fabricaton cost is much lower as a result of easy material deposition and patterning steps; the OFETs-based electronic devices could use plastic as substrates, therefore they would be very flexible and sometimes even transparent.[2] Till now OFETs have been integrated in application prototypes including flexible electronic paper,[5] OLED displays as driving elements,[6] and flexible radio-frequency identification (RFID) tags.[7] While promising future markets in consumer electronic device area are opened up, most of them have yet to reach mass production stage.[8,9] At this moment, OFETs are still being extensively studied to better understand the charge transport physics, especially in the newly reported high performance polymers, to further improve their performance and push OFETs toward large-scale production in the future.

My study will focus on the charge transport physics in OFETs with a recently reported high electron mobility polymer, poly{[N,N'-bis(2-octyldodecyl)-naphthalene-1,4,5,8-bis(dicarboximide)-2,6-diyl]-alt-5,5'-(2,2'-bithiophene)} (P(NDI2OD-T2). In this chapter, I will give an introduction firstly to the electronic structure of semiconducting polymers followed by the operating principles of OFETs; next, the charge transport models, the charge modulation spectroscopy (CMS) technique, and CMS results of P(NDI2OD-T2) from literature; at last, my motivation and scope of this study.
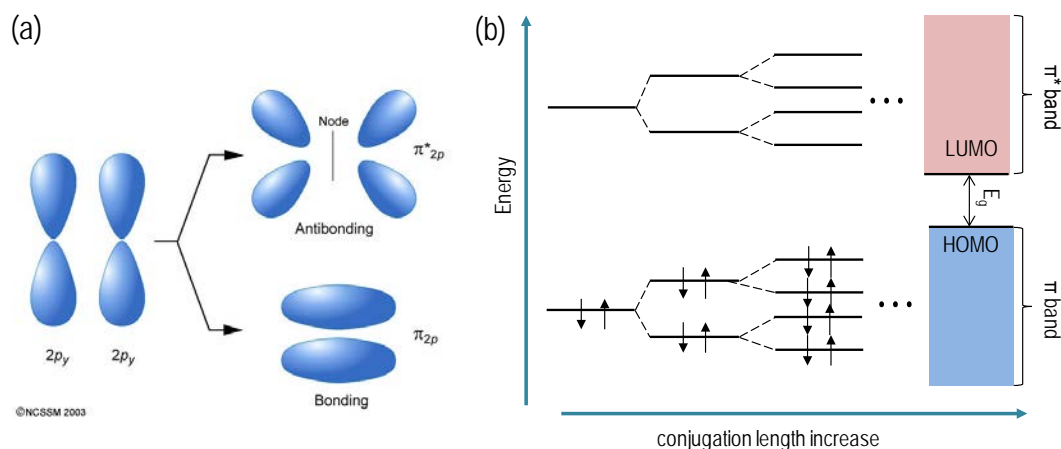
1.1   ORGANIC SEMICONDUCTORS

Figure 1.1: (a) π-orbital formation by carbon 2pz orbitals overlapping, from Ref [10], together with (b) illustration of the π and π* band formation of with increased conjugation length, with indicated HOMO, LUMO energy levels and the band gap (Eg).

Organic semiconductors can be divided into small molecules and polymers. Small molecules generally have several fused benzene and/or thiophene rings while polymer chains extend much longer with large number of repeating units or monomers. The alternating single and double carbon bonds in organic semiconductors lead to the overlapping of $2p_z$ orbitals between adjacent carbon atoms to form π and π* orbitals. When the conjugation level increases, the energy levels of π and π* orbitals split and start to form the π and π* band as shown in Figure 1.1, with band gap (E_g) between the highest occupied molecular orbital (HOMO) and lowest unoccupied molecular orbital (LUMO). The band gap leads to the semiconducting properties of these materials, enabling them to transport charges, as well as the light emitting properties at certain wavelength ranges with molecular structure and band gap engeering.[4]

1.2   ORGANIC FIELD-EFFECT TRANSISTORS

The first OFET based on polyethylene was first reported in 1986,[11] and along the years, OFETs have greatly improved in their performance and reliability. Now, the performance of OFETs are comparable to amorphous silicon (a-Si) transistors with field effect mobilities of 0.5–1 cm2/V s, and some high performance polymers were reported to have mobility even at 1–10 cm2/V s.[2,12]
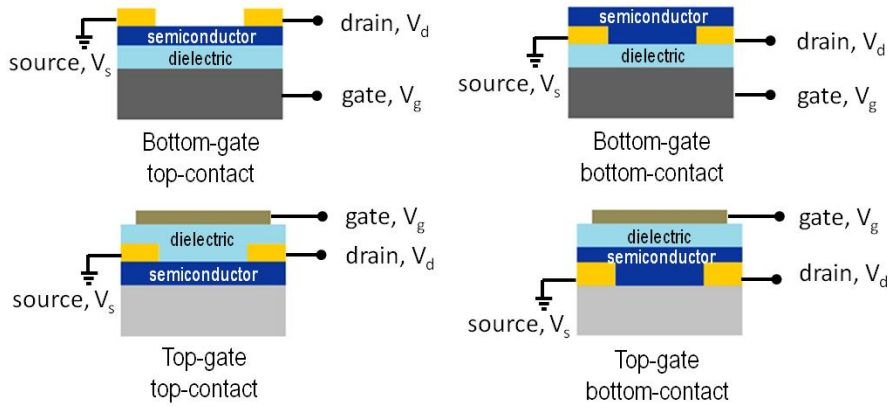
2

1.2.1 DEVICE STRUCTURE

Figure 1.2: Commonly used OFET device configurations

Field-effect transistors are three terminal devices with source, drain, and gate contacts, plus the organic semiconductor layer and gate dielectric layer. The four common configurations are shown in Figure 1.2, differing in relative placement of the gate and source-drain electrodes with respect to the semiconductor and gate dielectric layers. Each configuration offers its unique advantage. For example, in the bottom-contact configurations the source-drain electrodes are deposited prior to the semiconductor layer and naturally would not cause any damage to it. Also in top-gate structures, the top gate electrode and gate dielectric layer can provide effective encapsulation of the semiconductor layer against air and moisture in environment.[13] Moreover, the device configuration affects the charge carrier injection. The staggered structures (top-gate bottom-contact and bottom-gate top-contact) offer lower contact resistance as charge carriers can access the channel from a larger area of the source and drain electrodes.[14]

1.2.2 WORKING PRINCIPLES

When a gate voltage (V_g) is applied on the transistor, holes or electrons accumulate at the semiconductor/dielectric interface in the channel between the source and drain electrodes depending on the polarity of the voltage. The carrier concentration can be calculated based on the capacitance of the dielectric layer, which is $C = k\varepsilon_0/d$, where ε_0 is vacuum permittvity, k is the dielectric constant, and d is its thickness. The accumulated charge carriers will move when source drain voltage V_d is applied to form a electric field across the channel.

Under gradual channel approximation, the *I-V* characteristics of field-effect transistor can be expressed as

$$I_{sd} = \frac{\mu C W}{L}\left((V_g - V_{th})V_d - \frac{V_d^2}{2}\right)$$ (1.1)

where μ is the field-effect mobility, C is the capacitance (unit: F/m² or nF/cm²), L and W are the channel length and width respectively, and V_{th} is the threshold voltage for gate bias.[15] Charge carrier mobility is assumed same along the channel and the contact resistance negligible. V_{th} comes from charge trapping in localized states at the semiconductor-dielectric interface.

In the linear regime where $\left|V_g - V_{th}\right| \gg |V_d|$, the equation can be approximated to be,

$$I_{sd} = \frac{\mu C W}{L}(V_g - V_{th})V_d$$ (1.2)

At certain V_g, $|V_d|$ increase leads to carrier density decrease in the channel. When $|V_d|=|V_g-V_{th}|$, the carrier density near drain contact becomes zero, the source-drain would remain unchanged when $|V_d|$ further increases. The current in this saturation regime, where $|V_d| \gg \left|V_g - V_{th}\right|$, is approximated as,

$$I_{sd} = \frac{\mu C W}{2L}(V_g - V_{th})^2$$ (1.3)

The above current-voltage relationships assume ohmic contacts at the source and drain electrodes, with no potential drop at the electrodes for charge injection.

1.3 CHARGE TRANSPORT IN CONJUGATED POLYMERS

Conjuated polymers remain non-conducting in the absence of mobile charge carriers. Upon injection of excess charges into the π-conjugated system, charge transport occurs along the conjugated polymer chain direction and also across adjacent polymer chains.[16] Due to the complex molecular nature of such materials, several charge transport models were proposed to explain the charge transport in these materials, depending on the degree of structural order resulting from dfferent polymer structures and various processing conditions.[17]

1.3.1 MULTIPLE TRAPPING AND RELEASE MODEL

For organic semiconductors with sufficiently low degree of disorder, the multiple trapping and release (MTR) model, also called the mobility edge (ME) model, may be used to describe field-effect mobility as a function of gate voltage and temperature. In the MTR model,[18] charge carriers are trapped by impurities or in defects in low energy localized states. Upon thermal activation, the localized charge carriers are excited above the band edge into the charge transporting band which is normally described by free electron gas model. The band edge is described as mobility edge, below which charge carrier mobility is assumed to be zero, while above which the mobility is constant. The charge carriers would transport for some distance before they are trapped again in the trapped states as described in Figure 1.3.
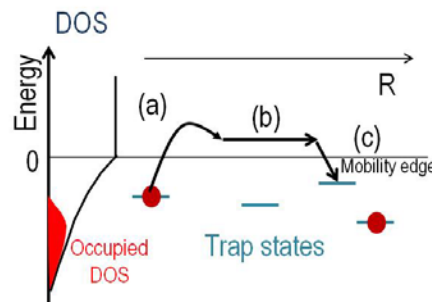

Figure 1.3: Multiple trapping and release model

The MTR model predicts an Arhennius-like temperature dependence of mobility at high temperature:

$$\mu = \mu_A \exp\left(-\frac{E_a}{kT}\right) \qquad (1.4)$$

where μ_A is an experimentally-determined pre-factor and E_a is the thermal activation energy of the field-effect mobility.

1.3.2 HOPPING MODELS

Charge transport in a disordered polymer system can also be modelled as charge hopping between localized states on transport sites. The hopping transport of charge carriers is usually understood in terms of the energy differences between transport sites and charge hopping rates,[19,20] and is dependent on the relative contributions of energetic disorder and polaron relaxation.[17]

Variations in intermolecular distances and conformational order in an amorphous polymer thin film limit the extent of delocalization of the charge carrier wavefunction across the film. The polymer chain is separated into shorter segments of conjugation lengths (lengths of defect-free oligomers) within which charge carriers are localized.[21] In addition to structural disorder, charge carriers are also localized by polarization. Within the near vinicty of a free charge carrier, the polymer lattice exhibits electronic and structural relaxation. The charge is self-trapped by the deformation it induces in the lattice, resulting in a polaron.[22]

The Gaussian Disorder Modelis commonly used to study the charge carrier mobility in amorphous organic materials.[19] Transport sites are subject to a Gaussian distribution of energies. Upward jumps to a higher energy state are thermally activated (Figure 1.4a), while downward jumps to a final lower energy state (Figure 1.4b) emits a phonon in the process.
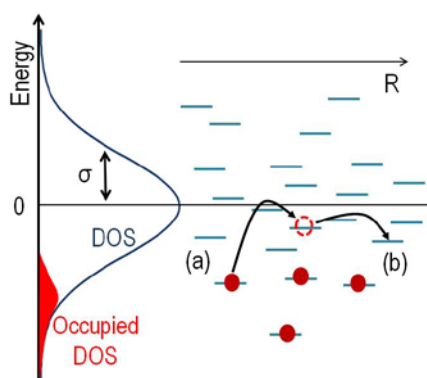

Figure 1.4: Charge transport by variable-range hopping by Gaussian disorder model (GDM)

However, disorder models including the GDM are based on the Miller-Abrahams hopping rate that neglects the more microscopic considerations of polaronic effects, such as the reduction of site energy due to polaronic relaxation.

The polaronic hopping model takes into consideration the lattice deformation giving rise to polaron binding energy or reorganization energy that influences charge transport. In a one-dimensional system, small polaron transport is modelled by Holsteinas independent events of hopping.[23] When a carrier is localized on a molecule, the electron energy level of the molecular site is lowered with respect to a neutral molecule. In order for the polaron to hop to another molecule, the lattice of the intial and final molecular sites has to be distorted such that the two local electronic energy levels achieve momentary energy degeneracy.

With regards to understanding experimentally derived properties of charge transport, the disorder hopping model is preferred over the polaron transport model, as disorder is still significant over a large temperature range.[24.,25] However, evidence of delocalized polarons have been observed in high mobility polymers.[17,26] The nature of such polarons will be further discussed in section 1.4.1.

1.4   Charge Modulation Spectroscopy

Experimentally, polaronic behaviour in charge transport is often masked by the effects of disorder. Charge modulation spectroscopy (CMS) is one technique that is able to provide experimental evidence that charge carriers are of a polaronic nature. Using electrical excitation of polymer-based thin film transistors, charge carriers are introduced by charge injection for optical probing, allowing a greater sensitivity to polarons in the charge accumulation region.

1.4.1   Polarons and Bipolarons

Polaron relaxation in the neutral ground state causes a downward shift in the LUMO and an upward shift in the HOMO in the ionized state. A hole polaron has a singly occupied lower energy level, while the electron polaron has filled lower energy levels with a singly occupied higher energy level. Figure 1.5 shows a diagram of the energy levels of a neutral polymer chain (left). By injecting an electron to the LUMO, a negatively charged polaron is formed and two new electronic states (polaronic levels P1 and P2) appear **deep in the π-π*** gap of the polymer. Similarly, a positively charged polaron is formed by removing an electron from the HOMO of the polymer.[27]
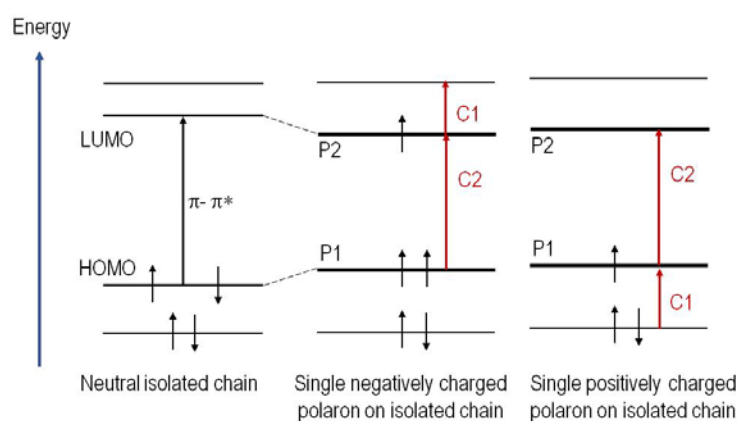
Figure 1.5: Energy diagram of neutral and singly charged polarons on a 1-D defect-free isolated chain

Depending on the structual order within the polymer, the polaron might not be confined to a single chain, but delocalized over a few polymer chains with strong interchain interactions. Existing polaronic levels are now split by the intermolecular interaction and consequently, new optical transitions are possible. The energy level schematic of a negatively charged polaron delocalized over two cofacial chains is shown in Figure 1.6.

Figure 1.6: Energy diagram of neutral isolated chain (left), and singly charged polaron on an isolated chain (middle) and delocalized over a cofacial dimer (right)

Because of the lattice distortion, another similar charge can be attracted to share the lattice distortion, forming a bipolaron. Bipolarons may also be formed via the recombination of polarons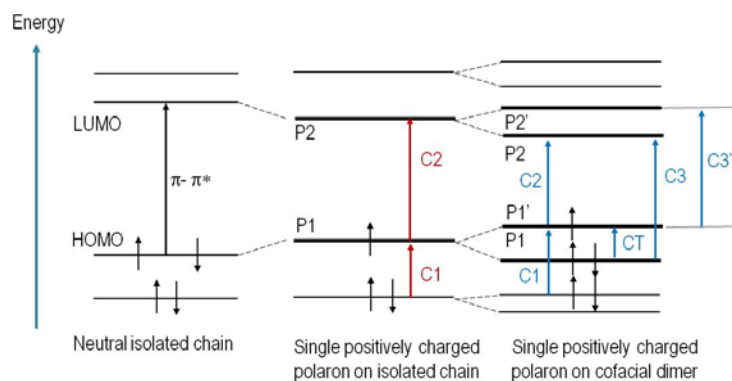.[28] In actual semiconducting polymer systems, the polymer chain first saturates with polarons before the formation of bipolarons at higher doping levels.[29]

1.4.2 WORKING PRINCIPLES

Polaron relaxation can be detected as charge-induced optical transitions at the conducting channel using CMS. If neutral polymer chains are ionized, the absorption transitions possible in the neutral polymer decrease and bleaching features are observed.

At a given wavelength of light incident on the OFET device, the gate voltage applied to the OFET device would be suitably high to induce charge accumulation at the conduction channel at the interface. In thin film transistors, mobile carriers are concentrated in the interface region within a few nanometers thickness.[21] A positive gate bias would induce electron and negative gate bias would induce hole carriers. A sinusoidal alternating voltage would be superimposed on the non-zero constant gate voltage to vary the concentration of charge carriers induced. At the point of the voltage modulation where the gate bias applied across the device is the largest, charge accumulation is at a maximum.The change in the intensity of light reflected when the charge concentration peaks is measured. Each measurement can be expressed in two components: the in-phase component in sync with the modulating gate bias, and the out-of-phase or quadrature component. If the measured signal reflects only the effects of the modulated gate bias, it will be of the same phase at each wavelength and therefore it can be rotated into phase by a constant phase shift angle with minimal quadrature components.

1.4.3 P3HT CASE STUDY

Poly(3-hexylthiophene) (P3HT) is a *p*-type thiophene-based polymer semiconductor first synthesized by Rick McCullough in 1992.[30] P3HT is widely studied for understanding charge transport due to its high carrier mobility as a function of regioregularity. Hole field-effect mobilities of μ~10^{-5} cm^2/V s were reported for the first P3HT-based OFET device, but mobility values of up to 0.1–0.3 cm^2/V s could be achieved by using rr-(regioregular-) P3HT. [31]

Different synthesis and control conditions influence the extents of regioregularity in P3HT.[32] For high regioregularity, rr-P3HT polymer molecules are π–stacked in an in-plane direction giving an ordered lamellae packing structure (Figure 1.7c). The two-dimensional conjugated lammellae of the rr-P3HT molecules were found to allow efficient interchain charge transport, thus resulting in higher mobility values. Charge modulation spectroscopy (CMS) measurements of P3HT thin film devices gave direct evidence of the polaronic behaviour of charge carriers in the semiconductor.

The CMS spectra of amorphous, more regiorandom P3HT thin film transistors (Figure 1.7b and c) showed two broad charge-induced bands at 1.8 eV and below 1 eV, attributed to singly charged polarons and bipolaron transitions respectively, with the relevant energy diagrams in Figure 1.8a.[34] Carriers in regiorandom P3HT are concluded to be more confined to isolated chain segments. In comparison, optical transitions from the CMS absorption spectrum of rr-P3HT (Figure 1.9) could only be explained by taking into account interchain interactions.[31] There was observed a new C3 charge-induced transition in rr-P3HT close to the π–π* transition at 1.65eV (Figure 1.9a), as well as a pronounced low-energy charge transfer (CT) transition in the mid-infrared region (Figure 1.9b) at energies below 0.3eV.[54] These two additional transitions indicate polaron interchain delocalization, with similar characteristic energy levels as a dimerized polaron in Figure 1.6.

The above disucssed characteristic absorption features reveal that although the carriers in the ordered P3HT still have a polaronic nature, requiring their wavefunctions to be localized, they have a pronounced interchain character. The presence of strong π-π interchain interactions in rr-P3HT thus allows the delocalization of carriers over neighbouring chains.
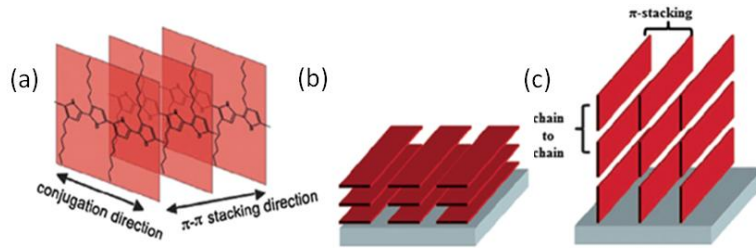
Figure 1.7 from Ref [33]: Schematic illustration of conjugated polymer molecular packing structures: (a) 2-D lamellae stacking; (b) face-on orientation and (c) edge-on oreintation of polymeric crystallites, with the π-stacking and the chain to chain packing of polymers
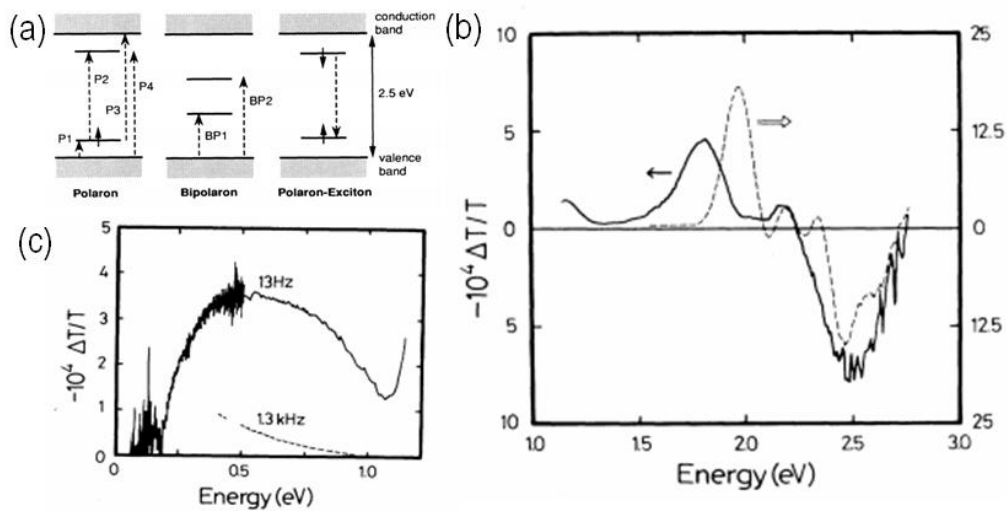
Figure 1.8 from Ref [34]: (a) Energy diagram and optical transitions of the different neutral and charged species of P3HT; Voltage modulated absorption spectra (f = 13 Hz) of (b) optical transmission (left), (Vg = range, ΔVg = 20 V ac), and (c) infrared transmission (Vg = 0±40 V above 0.5 eV and Vg = range, ΔVg = 40 V ac below 0.5 eV)
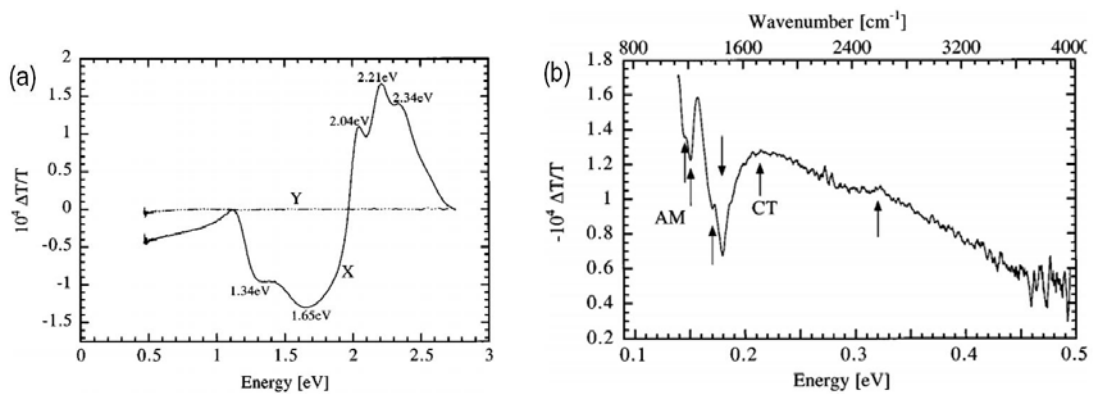
Figure 1.9 from Ref [31]: CMS absorption spectra (a) of P3HT in (f = 13 Hz, Vg = 0±1 V) with normalized in phase spectrum X and quadrature signal Y (b) in mid-infrared range (signal average of difference spectrum between Von = -30 V and Voff = +5 V)

1.5   POLYMER P(NDI2OD-T2)

Complementary metal-oxide semiconductor (CMOS) with low power consumption and stable operation necessitates both p-channel and n-channel materials that are reliable and high-performing. Many high-performing semiconductors are p-channel materials with majority charge carriers as holes, including regioregular poly(3-hexylthiophene) (P3HT), and poly(2,5-bis(3-hexadecylthiophen-2-yl)thieno[3,2-b]thiophene) (PBTTT).[12] Negative charge carriers are more likely to be trapped by common chemical impurities in the ambient environment, as well as hydroxyl, silanol, or carboxyl groups in common gate dielectric materials.[35]

In 2009, Fachetti et al. reported the excellent device performance and ambient stability of an electron-transporting n-type polymer, named poly{[*N,N'*-bis(2-octyldodecyl)-naphthalene-1,4,5,8-bis(dicarboximide)-2,6-diyl]-*alt*-5,5'-(2,2'-bithiophene)} (P(NDI2OD-T2), Polyera ActivInk N2200).[36] (P(NDI2OD-T2) comprises of alternating naphthalenediimide (NDI) acceptor and a dithiophene donor units. It has HOMO and LUMO levels at 5.6 eV and 4.0 eV below Fermi level.[36] The chemical structure of P(NDI2OD-T2) is shown in Figure 1.10.
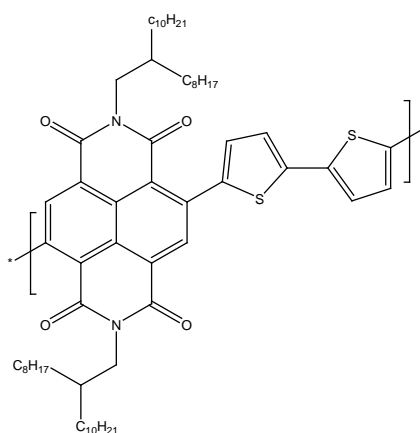
Figure 1.10: Chemical structure of P(NDI2OD-T2)

P(NDI2OD-T2)-based OFET devices could achieve mobilities from 0.1 to 0.8 cm^2/V s, across different solvents used, with a range of gate dielectrics, and multiple deposition techniques. [36] At the molecular level, studies have shown that the interconnectivity between crystalline and amorphous regions in the P(NDI2OD-T2) film from the overlapping layers in the face-on direction might have contributed to its high electron mobility.[37]

In addition, higher mobilities were found to be correlated to the larger extent of order and greater length of fibril-like structures observed in P(NDI2OD-T2) films using DCB and toluene as solvents compared to films using CN:CF. CMS measurements were made on P(NDI2OD-T2) films deposited by CN:CF, DCB and toluene. However, all three CMS absorption spectra showed identical polaronic and bleaching features, indicating that the charge carriers were similarly localized in all cases. It was concluded that the different field-effect mobility obtained using the three solvents did not result from the local packing of the polymer chains due to the common highly localized nature of polarons observed.[38]

The performance of P(NDI2OD-T2) based OFETs also appeared to be largely independent of gate dielectric constants within the range of more practical and commonly used polymer gate dielectrics.[36,37] Due to the long side chains in P(NDI2OD-T2), the backbone of the polymer chain is separated from the semiconductor-dielectric interface, and the effect of dipole disorder in the gate dielectric film is negligible. However, over a large range of $k = 2.6$ to $k = 7.8$, carrier mobility was found to be reduced and activation energy for field-effect mobility was found to increase with increasing k.[39] Caironi et al. found a strong dependence of the field-effect activation energy on the type of gate dielectric used. OFETs with CYTOP had a significantly lower activation energy (44 meV) compared to PS (64 meV) and PMMA (86 meV).[37]

1.5.1 CMS Study of P(NDI2OD-T2)-based OFETs

Previous investigations have employed CMS measurements on P(NDI2OD-T2)-based OFETs, and from observations of the charge-induced absorptions obtained, concluded that there is low energetic disorder on the interface inhibiting the transport of localized charges.[37,38,40] From Figure 1.11, a broad bleaching peak (from 1.5–2.0 eV) was identified as the bleaching of the ground state neutral polymer chain absorption. Two absoption peaks were identified as characteristic charged-induced absorption at 1.48 eV and ~2.8 eV, from which the lower energy absorption had well-defined features, suggesting that the energy distribution of charges are within a narrow range.[37]

In another study, an additional charge-induced absorption peak at ~1.6 eV was more clearly observed at low temperature of 100 K. At room temperature, the 1.6 eV peak was only evident from a dip or valley in the bleaching region but became more pronounced at low temperatures

(Figure 1.12). The authors eventually consigned the new absorption band to originate from the same charged polymeric segment as the 1.45 eV peak. [40]

The CMS measurements have also been compared with quantum-chemical simulations to understand the spectral features involved. The two main absorption bands observed were consistent with time dependent density functional theory (TDDFT) calculations of a negative singly charged and isolated polymer chain with four repeat units. The authors subsequently inferred that charge transport in P(NDI2OD-T2) is via polarons in the absence of interchain interactions.

Finally, the authors of the first study singled out the low energy absorption peak for comparison among different gate dielectrics used in Figure 1.13. With increasing k of the gate dielectric used, the polaron peak was observed to have broadened and shifted to lower energies, giving a more localized polaron on the polymer chain.[37]
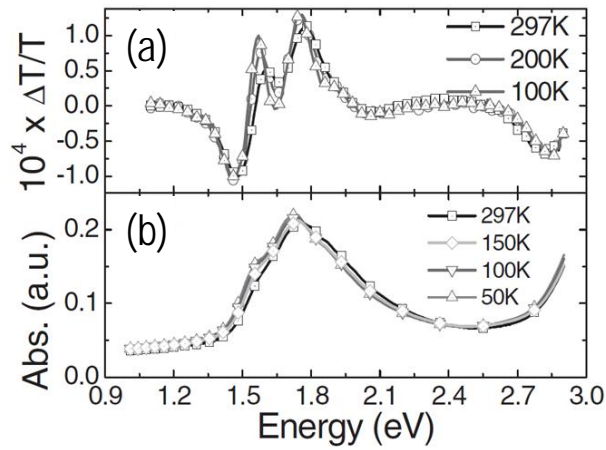
Figure 1.11 from Ref [37]: (a) Variable temperature CMS spectrum of P(NDI2OD-T2)-based OFET with CYTOP (f = 37 Hz, Vg = 20±5 V) (b) P(NDI2OD-T2) thin-film absorption spectra as functions of temperature
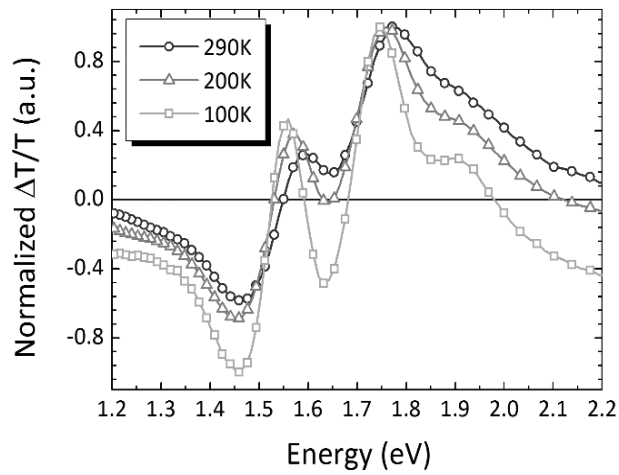
Figure 1.12 from Ref [40]: Variable temperature CMS spectra of P(NDI2OD-T2) based normalized to the central bleaching peak at 1.77 eV (f = 1127 Hz, Vg= 60 ±25 V)

Figure 1.13 from Ref [37]: Effect of the gate dielectric on CMS spectra, normalized to each device capacitance.

1.6 PROJECT MOTIVATION

In an OFET, the non-conducting gate dielectric layer separates the gate electrode and the organic semiconductor layer. The gate dielectric layer should give a high capacitance and remain defect-free to avoid trapping states, with a substantial dielectric breakdown threshold to give low gate leakage such that a higher density of charge carriers can be accumulated when the OFET is in operation.[7] In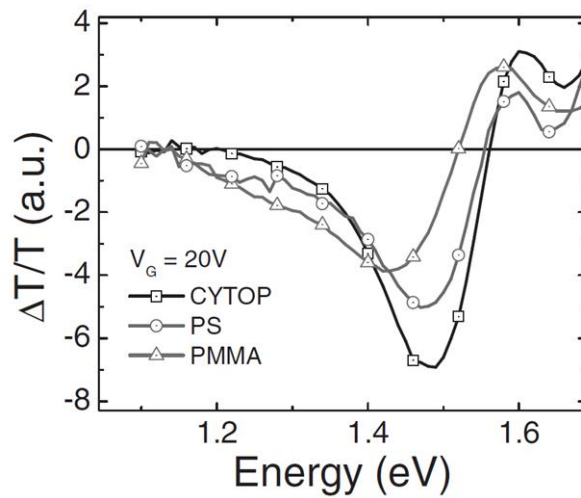 addition, the dielectric influences the morphology and the degree of order of the organic semiconductor at the interface.[17]

While a large dielectric constant is desirable in the dielectric constant to induce high charge carrier densities, the surface energy and disoder induced by polar groups at the interface also affects device performance. Veres et al. observed that the field-effect mobilities of semiconducting polymers are higher in contact with low-k gate dielectrics compared to those with higher gate dielectric constant $k.$ The dielectric polymers with high k usually contain polar functional groups that results in a higher energetic disorder at the interface. The broader distribution of DOS increases charge carrier localization and lowers charge carrier mobility.[41]

Currently, the CMS technique has been employed to study the effects of semiconductor solvent and temperature on polaronic behaviour in P(NDI2OD-T2). An in-depth investigation of the use of different gate dielectrics as well as the resulting influence on the semiconducting polymer and its polaronic transport is still lacking.

The field-effect mobility in P(NDI2OD-T2)-based OFETs was found to be largely independent of the gate dielectric constant and thus disorder effects arising from the insulating layer. However, different semiconductor-dielectric combinations have led to different values of field-effect activation energy, suggesting that polaron localization increases significantly from CYTOP transistors to PS and PMMA. In order to have a better understanding of the relationship between the physical characteristics and electrical properties of P(NDI2OD-T2), we explore polaronic behaviour as a function of gate dielectric using CMS.

2 EXPERIMENTAL METHODS

2.1 DEVICE FABRICATION AND CHARACTERIZATION

2.1.1 IMAGE REVERSAL PHOTOLITHOGRAPHY

There are several methods to pattern souce/drain electrodes on glass substrates, including shadow evaporation through stensil mask, standard photolithography, and image reversal photolithography (IRL). The source/drain electrodes comprise of two layers: 7 nm chromium (Cr) at the bottom for adhesion purpose and 30 nm gold (Au) on top for charge carrier injection. The two layers should match in position and the electrode surface has to be flat to avoid possible electrical short problem from source/drain to gate electrode in top-gated devices.

The electrodes prepared by shadow evaporation often encounter the offset/misalignment problem between the two layers as shown in Figure 2.1, because the two metals sources are at different positions relative to the substrate. The severity of the problem depends on the relative position of the substrate to sources and thickness of the shadow mask (> 100 µm).
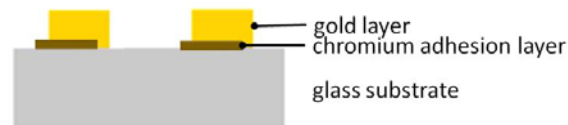
Figure 2.1: Illustration of the layer offset problem of source-drain metal electrodes by shadow evaporation

The electrodes prepared by standard photolithography often have shape edges due to the positive slope created during the masked UV exposure, illustrated in Figure 2.2. The metal evaporated onto the sidewall slope of the photo resist is unable to be removed during the lift-off step, leaving a "rabbit ear" profile. In contrast, negative sidewall slope can be easily created by image reversal photolithography (IRL). As a result, high quality electrodes are obtained, as shown in Figure 2.2, with flat top surface and no mismatch problem because of the thin photoreist layer (~ 1−2 µm) as compared to shadow mask.

Figure 2.2: Illustration of (a) positive slope problem in standard photolithography and (b) negative slope solution in reverse photolithography

Figure 2.3 shows the process of reverse image photolithography in detail as following: Glass substrates were cleaned with SC-1 solution (NH$_4$OH: H$_2$O$_2$: H$_2$O = 5: 20: 100) at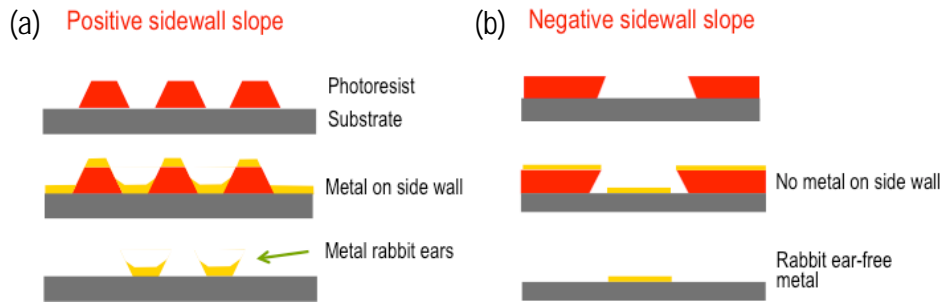 55–77°C for 30 minutes to remove particles, and then treated with hexamethyldisiloxane (HMDS) vapour at 120°C for 10 minutes to promote photo resist adhesion. The S1813 positive photo resist layer was spin coated at 3000 rpm to give film thickness of about 1.6 μm and annealed at 120°C for 3 minutes to remove solvent. Subsequently, the substrated was exposed to UV light using reverse mask for 40 seconds on Suss MJB3 Mask Aligner machine (Steps 1 and 2). The reverse mask is made of quartz with a thin metal layer to block light in the source/drain electrode region. After exposure, the substrates were treated in NH$_3$ vapor at 110°C for 5 minutes (Step 3) to remove the indene carboxylic acid generated by diazonaphthoquinone (DNQ), which functions as a dissolution inhibitor in the photo resist prior to UV exposure, to make the photoresist unsoluble outside source/drain region. After which, the substrates were flood exposed without mask under UV light for one minute (Step 4). The photo resist in the source/drain region were developed by immersing the substrates in the developer (95% water, 2.2% Tetramethylammonium hydroxide (TMAH)) for 2 minutes (Step 5), and the thin residual photo resist layers on the substrates were then etched off by short time oxygen plasma treatment (300 W, 0.4 min, Diener Oxygen Plasma Etcher, etching rate ~50 nm/min). Next, the 7 nm chromium and 30 nm gold metals were evaporated onto the substrates at a rate of about 0.1 nm/s in the BOC Edwards Thermal Evaporator at 10^{-6} mbar (Step 6). The photoresist was lifted-off using acetone to finish the photolithography process and we have the defined source-drain electrodes (Step 7).
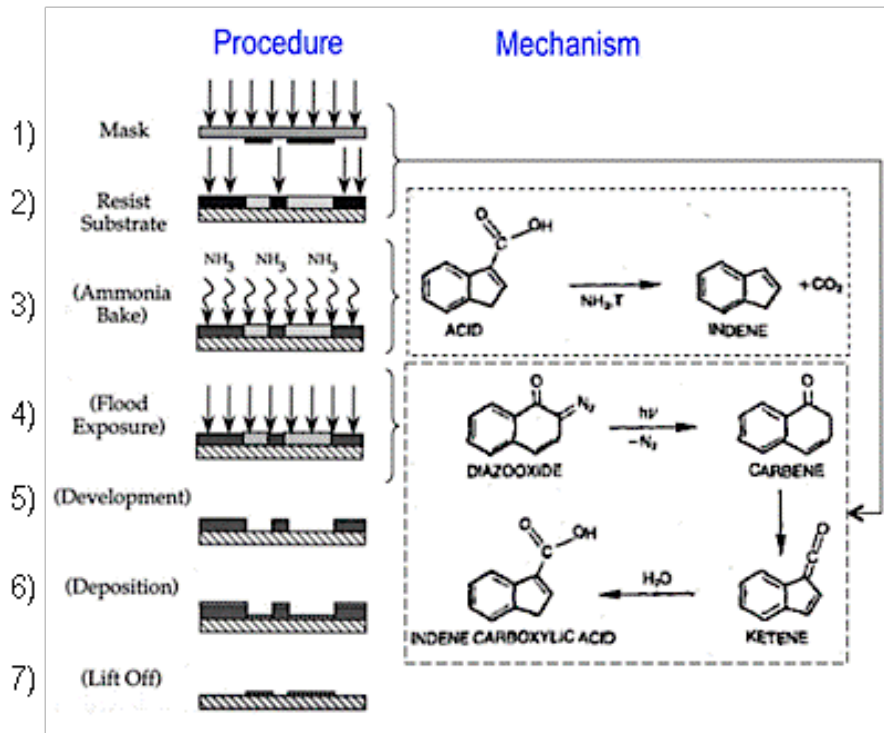
Figure 2.3 from Ref[42]: Illustration of reverse photolithography process

2.1.2 FET FABRICATION PROCEDURE

With patterned glass substrates (channel length L = 20 μm; channel width W = 22.5 cm), a 40-nm-thick poly{[N,N'-bis(2-octyldodecyl)-naphthalene-1,4,5,8-bis(dicarboximide)-2,6-diyl]-alt-5,5'-(2,2'-bithiophene)} P(NDI2OD-T2) (ActivInk N2200, Polyera) layer was spin-casted from pre-filtered (using PTFE 1 μm filter) 10 mg/ml chlorobenzene solutions in nitrogen-purged glovebox and annealed at 110°C for 10 minutes. Then the gate dielectric polymer was spin-coated on top, and annealed at 90°C for 30 minutes, with polymer structure and film thickness summarized in Table 2.1. At last, 7 nm chromium (Cr) and 30 nm silver (Ag) gate electrode layers were shadow evaporated to finish device fabrication.
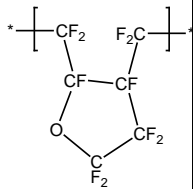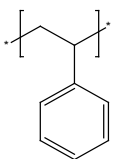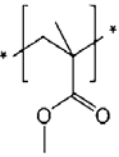
Gate Dielectric	Structure	k	Solvent	Thickness (±10 nm)	Capacitance (nF/cm²)
CYTOP (CTL-809M, Asahi Glass Chemical)		2.0	CT180 (Asahi Glass)	540	3.3
PS (2M MW , Polystyrene, Sigma Aldrich)		2.6	n-butylacetate	420	5.4
PMMA (960K MW , Polymethylmeth acrylate, Sigma Aldrich)		3.5	n-butylacetate	500	6.2

Table 2.1 Gate dielectric structures and thickness

The dielectric film thickness was chosen for the three dielectric layers to have similar capacitance values. Keeping the accumulated charge carrier concentrations similar in the devices during CMS measurements would make it easier to compare and interpretate results from different devices.

2.1.3 ELECTRICAL CHARACTERIZATION OF OFETS

The FETs were tested before they were taken to CMS measurements. The current-voltage (I-V) FET characteristics were collected in the nitrogen-purged glove box using a Keithley 4200 semiconductor parameter analyser. In the measurement process, the transfer curve was obtained by measuring source current I_s while sweeping V_{gs} from -10 V to 60 V (forward and back) at fixed source-drain voltage V_{ds}, which was stepped scanned from 0 V to 60 V at interval of 5 V. The output curve was obtained by sweeping V_{ds} from 0 V to 60 V (forward and back) at fixed V_{gs}, which was step-scanned from 0 V to 60 V at interval of 5 V. The gate leakage current was corrected by substracting off source-drain current I_s at $V_{ds} = 0$ V which comes solely from leakage through the gate dielectric layer ($\sim 10^{-6}$ A). Field-effect mobilities were extracted from the transfer curve in the linear regime where 50 V $< V_g <$ 60 V and $V_d = 25$ V. A large enough value of drain voltage is selected to minimize contact resistance induced mobility underestimation.

2.2 SPECTROSCOPY STUDY

2.2.1 ULTRAVIOLET-VISIBLE (UV-VIS) ABSORPTION SPECTROSCOPY

Borosilicate glasses were used as substrates. The P(NDI2OD-T2) and gate dielectric films were spin-coated and annealed with same conditions as those in FET devices described in section 2.1.2. Ultraviolet-visible (UV-vis) absorption spectrums were measured with the S1024DW Deep Well Spectrometer. During the measurement, a dark spectrum was first recorded which was subtracted away from subsequent reference and sample spectrum. The light from the deuterium and tungsten/halogen lamps were measured as the reference spectrum. Then the samples were placed in the light path and the corresponding spectrum was measured. The transmittance (T) was calculated from the ratio of the sample to the reference spectrum; the absorbance (A) could be calculated from transmittance as $A = -\log(T)$.

2.2.2 CHARGE MODULATION SPECTROSCOPY (CMS)

The top-gate bottom-contact FET devices were loaded into cryostat (Janis CCS-100/202) inside nitrogen-purged glove box and transferred to optical rig. During the transfer, the samples were protected with N_2 to minimize exposure to ambient environment, thus reducing device degradation and the resulting data inaccuracy. The cryostat was then pumped down to high vacuum (10^{-6} mbar) and the the device in vacuum was measured to ensure correct $I-V$ behaviour prior to charge modulation spectroscopy (CMS) measurement.
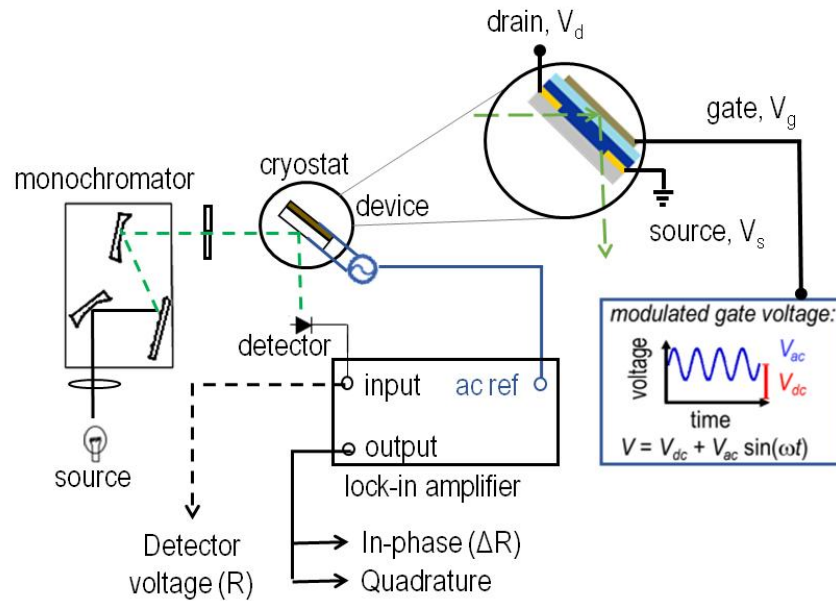
Figure 2.4: Schematic of CMS experiment set-up (simplified) in reflection mode

Figure 2.4 shows a schematic of the home-built experiment set up for the CMS measurement. Halogen lamp (50 Watt) was used as light source in the entire spectrum range (0.7 eV to 3 eV). Light comes out from light source passed through the monochrometer then was focused onto the iris where the light spot size can be adjusted. After that, the light beam was focused onto the interdigitated channel area from the glass substrate side of the FET device at ~ 45 degrees incident angle, and reflected off by the metal gate electrode. The reflected light was focused onto photodetector for the signal to be collected. Silicon photodetector was used in the visible range for photon energy above 1.2 eV and indium gallium arsenide (InGaAs) photodetector in the near infrared (NIR) range between 0.72 eV and 1.5 eV. The spectra collected via the two detectors in the overlapping energy range (1.2−1.5 eV) will typically match very well; the match would ensure that the rest of the experiment set up and the sample performance were stable during the entire measurement.

During the measurement, a constant source drain bias (V_d = 10 V and V_s = 0) and gate bias ($V_{g,DC}$ = 50 V) were applied on the device by high voltage amplifier (Avtech) to simulate a normal working device in the linear regime. Meanwhile, the carrier density in the channel was modulated at ω = 170 Hz by overlaying a sinusoidal gate bias ($V_{g,AC}$ = 10 V, peak value). The carrier density modulation led to a small modulation (ΔR, peak value) in the reflected light intensity (R) at same frequency, thus the small AC signal was picked up by the lock-in amplifier while R was measured by the Keithley 2400 sourcemeter. The two values were collected at energy step of 0.02 eV and were used to calculate the final $\Delta R/R$ CMS spectrum. Throughout the measurement, the whole CMS setup was covered to prevent any disturbance from environment, thus minimizing the noise level in the spectrum. Moreover, to improve the signal-to-noise ratio, each of the reported spectra was averaged over five spectra. *I-V* measurements were made before and after the CMS experiments to ensure that the devices were in normal condition throughout the experiments.

During data processing, the ΔR signal collected with lock-in amplifier would go through phase correction process, since the phase values of $V_{g,AC}$ and ΔR signal were generally different due to semiconductor properties and detector response. The phase difference (θ) would usually be constant through the whole spectrum range. In the phase correction, two sinosoidal reference signals with 90 degree phase difference were generated by the lock-in amplifier at the same modulation frequency; $V_{R1} = V_R \sin(\omega t + \phi_R)$ and $V_{R2} = V_R \sin(\omega t + \phi_R + \pi/2)$. Then they were multiplied with $\Delta R \sin(\omega t + \phi)$. For V_{R1} signal, the product was $\frac{1}{2} V_R \Delta R [\cos(\phi_R - \phi) - \cos(2\omega t + \phi_R + \phi)]$ and its DC part would be collected through a low pass filter as the in-phase component (X). Similarly, we could get the out-of-phase component (Y) to be $\frac{1}{2} V_R \Delta R \sin(\phi_R - \phi)$. The phase difference $\theta = \phi_R - \phi$ could be calculated from $\theta = \arctan (Y/X)$ while the ΔR value is proportional to $(X^2 + Y^2)^{1/2}$. Generally, ϕ_R would be adjusted to make θ equal to 0 and the corresponding X and Y would be plotted as the final data form.

To minimize the signals of irreversible processes in the measured spectrum (Appendix A), the magnitude of drain voltage applied across the conduction channels was optimized at V_d=10V. The use of a higher drain voltage at V_d=15V was found to have resulted in a non-zero quadrature signal when phase-corrected, possibly due to the higher gate leakage present in the device.

3 RESULTS AND DISCUSSION

3.1 FET CHARACTERIZATION

3.1.1 SOLVENT EFFECT

The device performance was optimized to provide a good starting point for CMS experiment. For the semiconductor layer, P(NDI2OD-T2) was spin-coated from dichlorobenzene (DCB) and chlorobenzene (CB) respectively to study the solvent effect. All the processing conditions were kept the same: the thickness of semiconductor layer was **around 30−40 nm**; P(NDI2OD-T2) films were annealed at 110°C for 10 minutes after spin-coating; PMMA was used as gate dielectric. The results showed that the CB device has linear mobility of 0.14 cm^2/V s while the DCB device has lower mobility of 0.036 cm^2/V s, as extracted from transfer curve of the two devices shown in Figure 3.1.
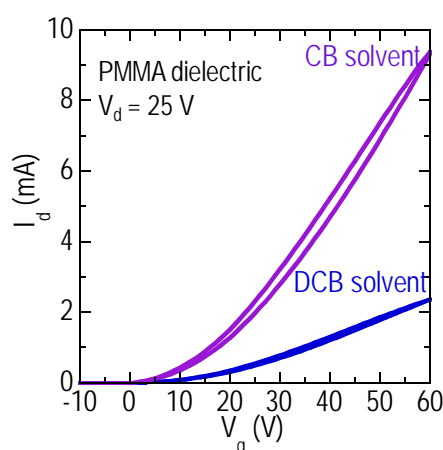
Figure 3.1: Comparison of P(NDI2OD-T2) top-gate bottom-contact transistors where the semiconductor layer was deposited from CB and DCB respectively. L = 20 μm, W =22.5 cm, C = 5.6 nF/cm².

The improved device performance could be related to the boiling point of the two solvents. Residual CB solvent in P(NDI2OD-T2) could be effectively removed by the 110°C annealing process due to its relatively low boiling point at 132°C. However, DCB has much higher boiling point between 174−180°C that makes it difficult to remove, thus compromising device performance. In addition, the degree of aggregation in P(NDI2OD-T2) solution was reported to be solvent dependent,[38] which could lead to different molecular packing structures in the film, giving rise to the performance difference.

Similarly for the polymer dielectric layer, the solvent removal was important since charge transport at the semiconductor/dielectric interface could be easily hindered by any residual solvent molecules. For PS and PMMA, the boiling point of *n*-butylacetate is low at 126°C thus the annealing time is kept short. But for CYTOP, the boiling point of its solvent is at 180°C thus we increased the annealing time to 30 minutes, which gave good results.

3.1.2 DIELECTRIC EFFECT

Figure 3.2 shows the transfer and output curves obtained from P(NDI2OD-T2) top-gate bottom-contact OFETs with different gate dielectrics at room temperature (300 K). The transfer curves were leakage corrected. All devices behaved well, with low threshold voltage, low hysteresis especially at low V_g and V_d bias, small contact resistance indicated by the clear take off at V_d = 0 V in output curves, and also low level of leakage current (~μA). In terms of source-drain current achieved with given V_g and V_d bias, CYTOP device was the best among all three devices, followed by PS device, then PMMA device. This was also reflected by extracted linear field-effect mobility given in Table 3.1.

From Table 3.1, the field-effect mobility, $\mu_{FET,}$ of P(NDI2OD-T2) was **between 0.1−0.3 cm^2/V s,** which is similar to literature reported values. The dependence of device performance at room temperature on dielectric constant is weak within the studied dielectric constant range. This was attributed to the long alkyl side-chains of P(NDI2OD-T2) which separate the polymer backbone from the semiconductor/dielectric interface by several Å to nm, effectively reducing the effect of dipole moments inside gate dielectric on charge transport along and between polymer backbones.[36]

At low temperature (200 K), all three devices still behaved very well, only with reduced current levels and slightly increased gate threshold voltage, indicating thermally activated charge transport behaviour. Nevertheless, the mobility spread between different devices became larger than that at room temperature. From the temperature dependence of mobility, the activation energy (E_A) of the FET devices were extracted by equation lnμ = −E_A/$k_B T$, where k_B is the Boltzmann constant and T is temperature. The results showed that E_A of the three devices had the following relationship: CYTOP < PS < PMMA, which were correlated to the dielectric constant.
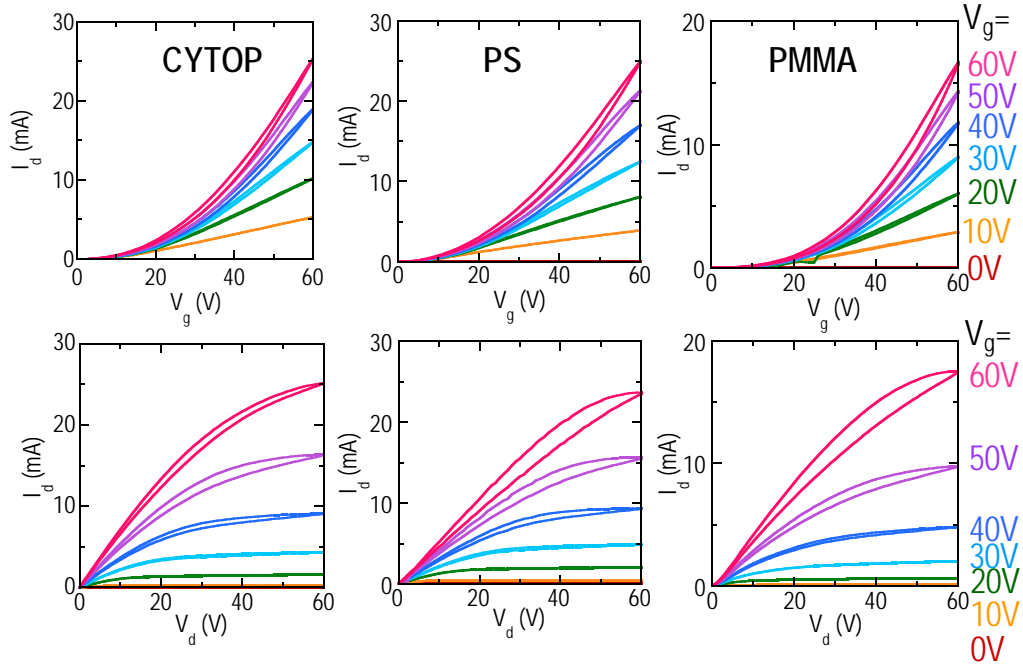
Figure 3.2: The transfer and output characteristics of P(NDI2OD-T2) top-gate bottom-contact transistors with three different dielectrics measured at room temperature. The transfer curves are all corrected for leakage current. L = 20 μm and W = 22.5 cm.

Gate Dielectric	k	μ_{FET}(cm^2/V s)		E_A (meV)
		295 K	200 K	
CYTOP	2.0	0.32	0.10	62
PS	2.6	0.13	0.030	78
PMMA	3.5	0.14	0.024	94

Table 3.1: The linear field-effect mobilities of P(NDI2OD-T2) top-gate bottom-contact transistors with different dielectrics at room temperature (295 K) and low temperature (200 K), also the activation energy of all three devices.

3.2 UV-VIS AND CMS MEASUREMENTS
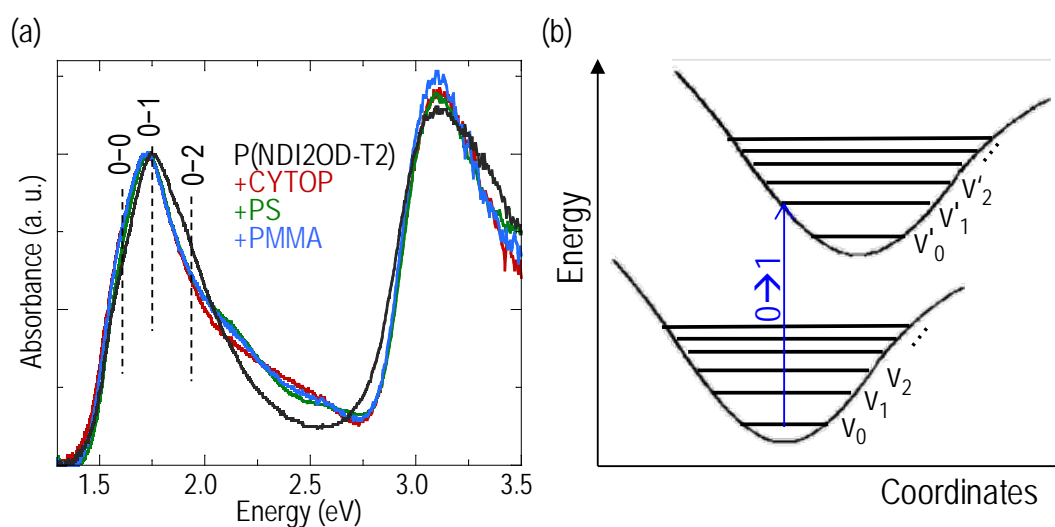
3.2.1 DIELECTRIC EFFECT

Figure 3.3: (a) UV-vis absorption spectrum of P(NDI2OD-T2) and P(NDI2OD-T2)/dielectric bilayer films. The spectrums were background corrected and normalized to 0−1 peak for comparison. (b) Illustration of the vibronic energy levels of molecules at ground and excited state; and the 0−1 electronic transition described by Franck−Condon principle.

The pristine P(NDI2OD-T2) film (Figure 3.3a) had two absorption maximum at ~1.75 eV and ~3.15 eV respectively. The thee vibronic features in the low energy region at 1.58, 1.75 eV and 1.92 eV had been assigned by previous authors to 0−0, 0−1 and 0−2 electronic transitions respectively from HOMO to LUMO of P(NDI2OD-T2) aggregate,[43] while the 3.15 eV peak in the highe energy region was assigned to 0−11 electronic transition from HOMO to LUMO+10 energy levels.[44] This "camel-back" characteristic of the absorption spectrum is due to the donor-acceptor nature of P(NDI2OD-T2). Quantum-chemical calculations have shown that the HOMO wavefunction localized on the bithiophene (T2) unit while the LUMO wavefunction localized on the NDI unit.[45] Charges transfer from the donor to acceptor unit during the HOMO to LUMO transition. The high energy π-π* transition from HOMO to LUMO+10 delocalized the wavefunction over several repeat units of the polymer chain.

The UV-vis spectrum of P(NDI2OD-T2)/dielectric bilayer films were similar to that of the pristine P(NDI2OD-T2) film with slight red shift of the 0−1 peak and decrease of the 0−2 shoulder. The similar 0−0/0−1 peak ratio indicated same degree of order in the P(NDI2OD-T2) film as described by the H-aggregate model.[46] Thus the dielectric layer did not affect the underlying semiconductor packing structure, regardless of dielectric constant and different processing conditions, such as solvent and annealing temperatures.
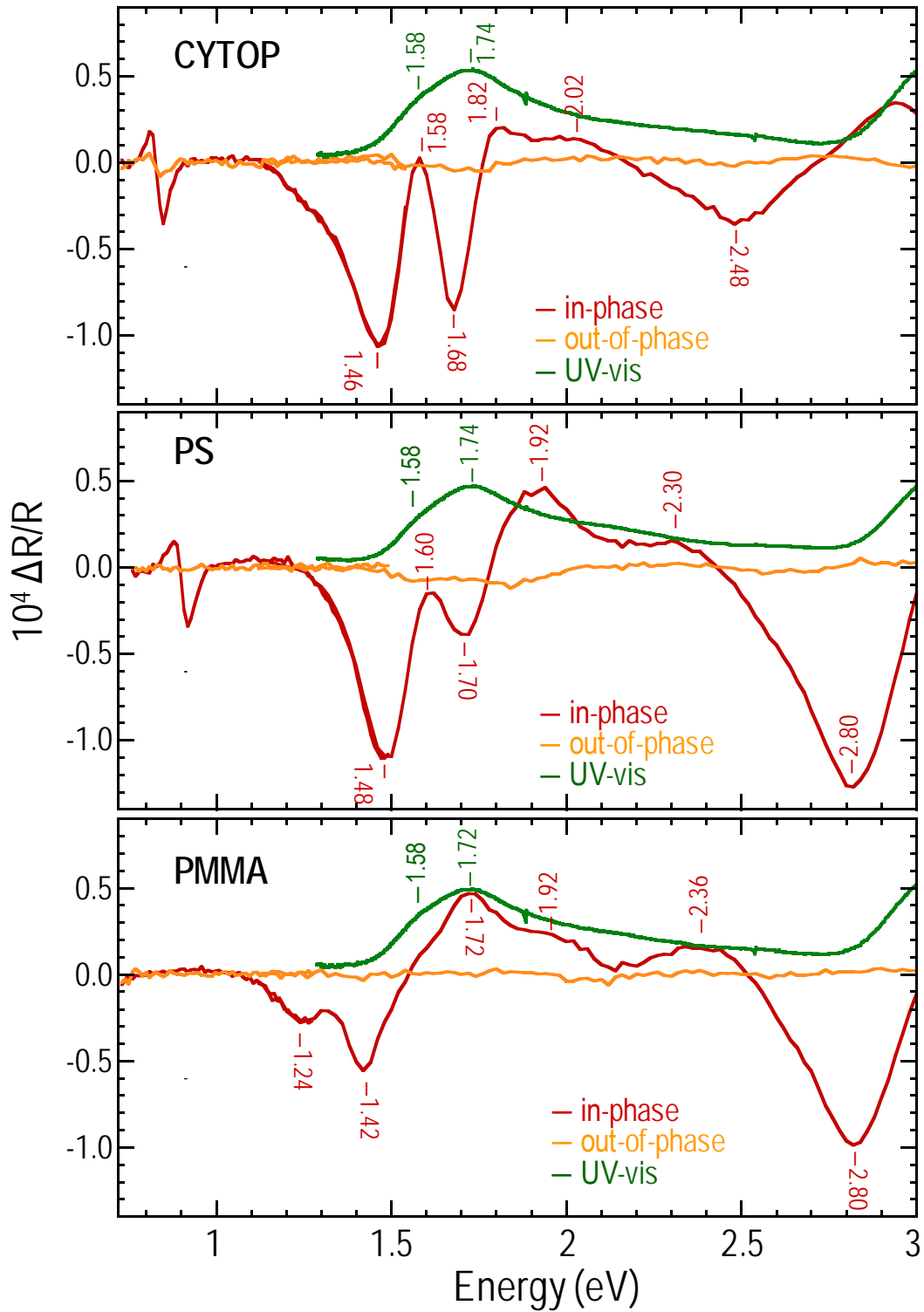
Figure 3.4: The CMS spectrum of P(NDI2OD-T2) top-gate bottom-contact transistors at room temperature (295 K) with three different dielectrics.The UV−vis spectrum are given for reference together with the peak positions of both CMS and UV−vis spectrum. Data collection conditions: f = 170 Hz, Vd = 10 V, Vg = 50±10 V.

Figure 3.4 shows the CMS spectra measured for P(NDI2OD-T2) top-gate bottom-contact transistors at room temperature (295 K) with three different dielectrics after phase correction. The results from both Si and InGaAs detectors were plotted together and they matched each other very well. The phase angle used for correction was constant in all devices and over the entire wavelength range; it only varied when different detectors were used. The spectrum of CYTOP and PS devices had roughly similar features while that of PMMA device was quite different. The large dependence of CMS spectrum of P(NDI2OD-T2) top-gate transistors on gate dielectrics, in contrast to the results from UV-vis measurements, correlated with the field-effect mobility and device activation energy variation with different dielectrics.

For CYTOP and PS devices, the CMS spectrum had narrow absorption peaks ($\Delta R/R < 0$) in low energy region at 1.46/1.48 eV (CYTOP/ PS) and 1.68/1.70 eV; a broad absorption peak in high energy region at 2.48/2.80 eV; also a broad bleaching band ($\Delta R/R > 0$) around 1.8−2.2 eV (CYTOP)/ 1.8−2.5 eV (PS). For PMMA device, the main difference was the absence of the absorption peak near 1.69 eV and the appearance of an absorption shoulder at 1.24 eV; also, the bleaching band extended to a lower energy of ~1.6 eV with a main peak at 1.72 eV matching the absorption maximum of the UV-vis spectrum.

The difference in the three spectrum was an effect of different degrees of carrier delocalization in P(NDI2OD-T2) film caused by gate dielectrics. Previous study showed that the dipole moment in gate dielectrics led to charge carrier localization;[41] therefore, the charge carriers in PMMA device were expected to be most localized while the carriers in CYTOP devices were most delocalized. The CMS spectrum was a mixture of signals from single polymer chain and aggregates.

The main absorption feature of single chain in the visible to near-IR region was the C2 transition which was assigned to the 1.42 eV peak in PMMA device and 1.48/1.46 eV peak in PS/CYTOP devices (see Figure 1.6 for transition labels). The larger C2 peak value in PS/CYTOP devices was a result of greater degree of carrier delocalization which caused the polaron level to be closer to neutral states. In the case of aggregates, the polaron level of single chains would split, giving rise to a new transition peak C3, which was observed in PS/CYTOP devices at 1.70/1.68 eV. The C3/C2 peak ratio reflected the proportion of contribution by the aggregates in the spectrum, and thus the carriers were more delocalized in CYTOP devices. The increase of charge carrier delocalization with decrease of dielectric

constant agreed with the dipole model, and was the direct reason for the smallest activation energy in CYTOP devices.

The bleaching band of PMMA device showed vibronic structure with peaks and shoulders at 1.58 eV, 1.72 eV, and 1.92 eV corresponding to the peaks in UV-vis spectrum. In contrast, the 0−1 bleaching peak (1.72eV) was absent in spectrum of PS and CYTOP devices while the 0−0 bleaching peak (1.58eV) was very low. This result came from supposition of the strong C3 absorption peak and the two bleaching peaks. As they were opposite in sign, the superposition led to the reduction of 0−0 peak height and absence of 0−1 peak since its energy was very near to the C3 peak. Nevertheless, the 0−2 bleaching peak at 1.92 eV was still observed in spectrum of PS device, confirming our hypothesis.

The results showed that dielectrics had strong effect on the charge transport in P(NDI2OD-T2) top-gate transistors by affecting the degree of carrier delocalization. Despite the difference in the three spectrums, all the bleaching peaks in low energy range were narrow in width comparing with the spectrums of common semiconducting polymers e.g. rr-P3HT[31] and PBTTT[47], indicating the low degree of disorder in P(NDI2OD-T2) thus its superior charge transport performance.

3.2.2 Temperature Effect

Figure 3.5 shows the CMS spectra obtained from P(NDI2OD-T2) top-gate bottom-contact transistors at room temperature (295 K) and low temperature (200 K) for all three different dielectrics after phase correction. Overall, the spectrums at high and low temperatures were quite similar in all the features, with slight position shifts and height variations for some peaks, consistent with literature report in which the spectrum of P(NDI2OD-T2) varied little even when the temperature was decreased to 100 K.[37]

The most prominent change in the low energy region of the spectrum was the increase of the 0−0 peak intensity for CYTOP and PS devices. The higher 0−0 peak intensity suggested higher degree of order in P(NDI2OD-T2) films at low temperature under reduced intensity of molecular vibrations. For the C2 absorption peaks, the peak positions of both CYTOP and PS devices shifted to 1.46 eV while that of PMMA device blue shifted to 1.44 eV.
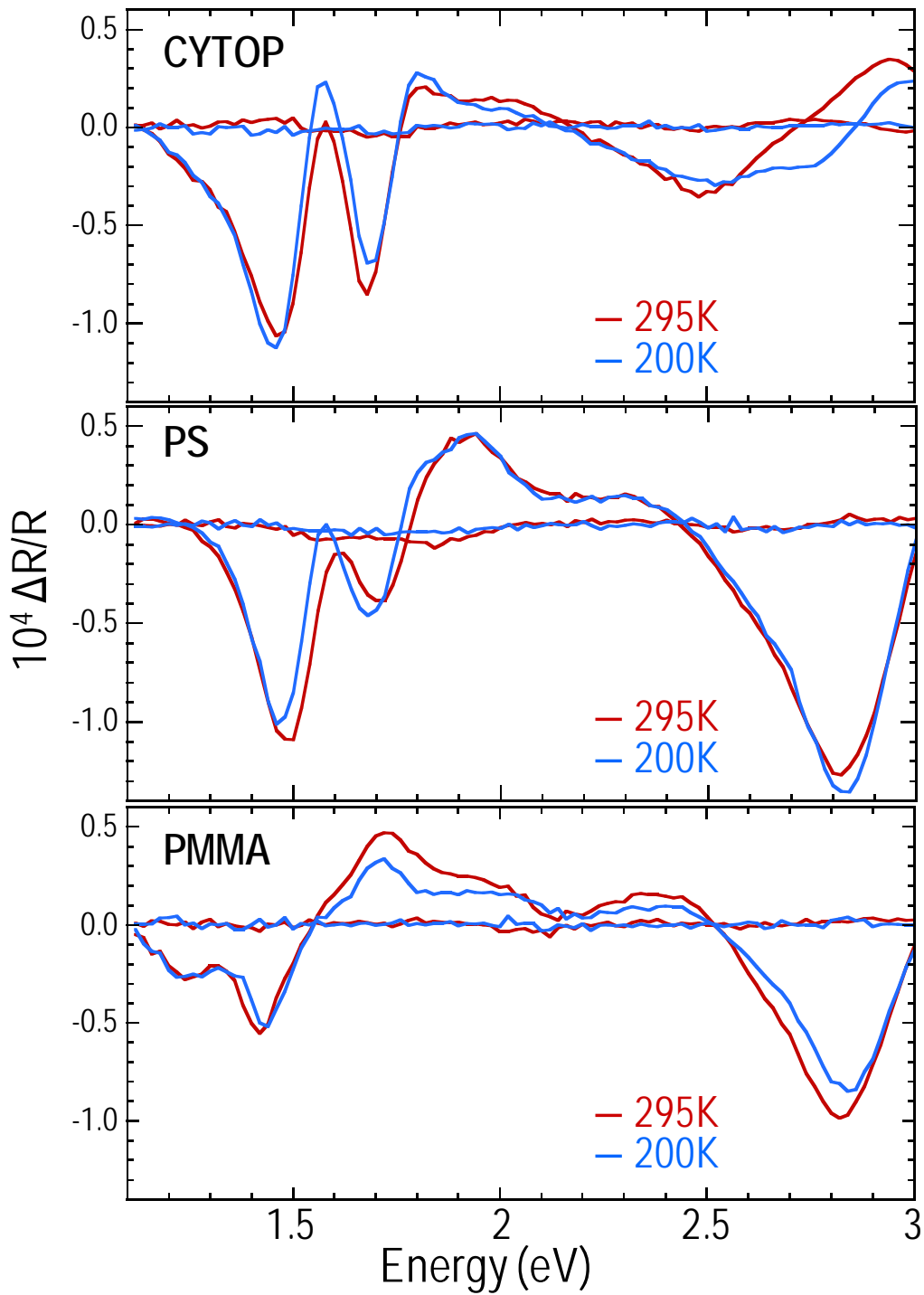
Figure 3.5: The CMS spectrum of P(NDI2OD-T2) top-gate bottom-contact transistors at room temperature (295 K) and low temperature (200 K) with different dielectrics. Data collection conditions: f = 170 Hz, Vd = 10 V, Vg = 50±10 V.

4   CONCLUSION

The nature of charge carriers in P(NDI2OD-T2), a good electron transporting n-type polymer, has been investigated via charge modulation spectroscopy (CMS). CMS measurements at room temperature revealed unique polaron characteristics of P(NDI2OD-T2) interfaced with different gate dielectrics in top-gate bottom-contact organic field-effect transistors (OFETs).

While common charge-induced polaronic absorption features were observed in the low energy region around 1.49 eV, the $\Delta R/R$ intensities of a separate absorption peak at 1.60 eV are correlated to the gate dielectric constant k used. The P(NDI2OD-T2) –based OFET device with CYTOP had the largest intensity of this higher energy absorption peak, followed by the transistor device with PS, but the device with PMMA had no observable absorption features at the same energy. While previous CMS studies of P(NDI2OD-T2) concluded that charges in the semiconducting film are localized on isolated polymer chains and are characterized by only intramolecular interactions, the CMS data from this project suggests possibilities of interchain interaction with need for further work in CMS spectral characterization in the mid-infrared (MIR) region to study possible C1 and CT transitions (see Appendix B for preliminary work).

Low temperature CMS measurements confirmed a decrease in mobile transport polarons leading to a decrease in field-effect mobility. Due to the complex spectral features arising from the overlap between the charge-induced absorption band and the bleaching band at very near energies, more detailed modelling and investigations into the molecular chemical nature of P(NDI2OD-T2) is required.

5 REFERENCES

1. Barbe, D. Surface state parameters of metal-free phthalocyanine single crystals. *Solid State Commun.* 8, (1970) 2679-2687.
2. Horowitz, G. Organic Field-Effect Transistors. *Adv. Mater.* 10, (1998) 365-377.
3. Li, G., Zhu, R. & Yang, Y. Polymer solar cells. *Nature Photon.* 6, (2012) 153-161.
4. Mitschke, U. & Bäuerle, P. The electroluminescence of organic materials. *J. Mater. Chem.* 10, (2000) 1471-1507.
5. Rogers, J., Bao, Z., Baldwin, K., Dodabalapur, A., Crone, B., Raju, V., Kuck, V., Katz, H., Amundson, K., Ewing, J. & Drzaic, P. Paper-like electronic displays: Large-area rubber-stamped plastic sheets of electronics and microencapsulated electrophoretic inks. *P. Natl. Acad. Sci. USA* 98, (2001) 4835-4840.
6. Sirringhaus, H. Integrated Optoelectronic Devices Based on Conjugated Polymers. *Science.* 280, (1998) 1741-1744.
7. Drury, C., Mutsaers, C., Hart, C., Matters, M. & de Leeuw, D. Low-cost all-polymer integrated circuits. *Appl. Phys. Lett.* 73, (1998) 108.
8. Sheats, J. Manufacturing and commercialization issues in organic electronics. *J. Mater. Res.* 19, (2004) 1974-1989.
9. Kelley, T., Baude, P., Gerlach, C., Ender, D., Muyres, D., Haase, M., Vogel, D. & Theiss, S. Recent Progress in Organic Electronics: Materials, Devices, and Processes. *Chem. Mater.* 16, 4413-4422 (2004).
10. Dlt.ncssm.edu. (2015). *TIGER - NCSSM Distance Education and Extended Programs.* Retrieved 26 March 2015, from http://www.dlt.ncssm.edu/tiger/chem3.htm
11. Tsumura, A., Koezuka, H. & Ando, T. Macromolecular electronic device: Field-effect transistor with a polythiophene thin film. *Appl. Phys. Lett.* 49, (1986) 1210..
12. Sirringhaus, H. 25th Anniversary Article: Organic Field-Effect Transistors: The Path Beyond Amorphous Silicon. *Adv. Mater.* 26, (2014) 1319-1335.
13. Noh, Y. & Sirringhaus, H. Ultra-thin polymer gate dielectrics for top-gate polymer field-effect transistors. *Org. Electron.* 10, (2009) 174-180.
14. Richards, T. & Sirringhaus, H. Analysis of the contact resistance in staggered, top-gate organic field-effect transistors. *J. Appl. Phys.* 102, (2007) 094510.
15. Horowitz, G. & Delannoy, P. An analytical model for organic-based thin-film transistors. *J. Appl. Phys.* 70, (1991) 469.

16. Basescu, N., Liu, Z., Moses, D., Heeger, A., Naarmann, H. & Theophilou, N. High electrical conductivity in doped polyacetylene. *Nature.* 327, (1987) 403-405.

17. Sirringhaus, H. Device Physics of Solution-Processed Organic Field-Effect Transistors. *Adv. Mater.* 17, (2005) 2411-2425.

18. Horowitz, G., Hajlaoui, M. & Hajlaoui, R. Temperature and gate voltage dependence of hole mobility in polycrystalline oligothiophene thin film transistors. *J. Appl. Phys.* 87, (2000) 4456.

19. Bässler, H. Localized states and electronic transport in single component organic solids with diagonal disorder. *Phys. Status Solidi B.* 107, (1981) 9-54.

20. Vissenberg, M. Theory of the field-effect mobility in amorphous organic transistors. *Phys. Rev. B.* 57, (1998) 12964-12967.

21. Bässler, H. Charge Transport in Disordered Organic Photoconductors a Monte Carlo Simulation Study. *Phys. Status Solidi B.* 175, (1993) 15-56.

22. Fishchuk, I., Kadashchuk, A., Bässler, H. & Nešpůrek, S. Nondispersive polaron transport in disordered organic solids. *Phys. Rev. B.* 67, (2003) 224303.

23. Holstein, T. Studies of polaron motion. *Ann. Phys.-New York.* 8, (1959) 325-342.

24. Van der Auweraer, M., De Schryver, F., Borsenberger, P. & Bässler, H. Disorder in Charge Transport in doped polymers. *Adv. Mater.* 6, (1994) 199-213.

25. Wohlgenannt, M., Jiang, X. & Vardeny, Z. Confined and delocalized polarons in π-conjugated oligomers and polymers: A study of the effective conjugation length. *Phys. Rev. B.* 69, (2004) 241204

26. Brédas, J. & Street, G. Polarons, bipolarons, and solitons in conducting polymers. *Acc. Chem. Res.* 18, (1985) 309-315.

27. Bertho, D. & Jouanin, C. Optical absorption from polarons and bipolarons in polythiophene. *Synthetic Met.* 24, (1988) 179-192.

28. Brédas, J., Cornil, J. & Heeger, A. The exciton binding energy in luminescent conjugated polymers. *Adv. Mater.* 8, (1996) 447-452.

29. Harbeke, G., Meier, E., Kobel, W., Egli, M., Kiess, H. & Tosatti, E. Spectroscopic evidence for polarons in poly(3-methylthiophene). *Solid State Commun.* 55, (1985) 419-422.

30. McCullough, R. & Lowe, R. Enhanced electrical conductivity in regioselectively synthesized poly(3-alkylthiophenes). *J. Chem. Soc. Chem. Comm.* 1 (1992) 70-72.

31. Sirringhaus, H., Brown, P., Friend, R., Nielsen, M., Bechgaard, K., Langeveld-Voss, B., Spiering, A., Janssen, R., Meijer, E., Herwig, P. & de Leeuw, D. Two-dimensional charge transport in self-organized, high-mobility conjugated polymers. *Nature.* 401, (1999) 685-688.

32. McCullough, R. The Chemistry of Conducting Polythiophenes. *Adv. Mater.* 10, (1998) 93-116.

33. Yao, Y., Dong, H. & Hu, W. Ordering of conjugated polymer molecules: recent advances and perspectives. *Polym. Chem.* 4, (2013) 5197.

34. Ziemelis, K., Hussain, A., Bradley, D., Friend, R., Rühe, J. & Wegner, G. Optical spectroscopy of field-induced charge in poly(3-hexyl thienylene) metal-insulator-semiconductor structures: Evidence for polarons. *Phys. Rev. Lett.* 66, (1991) 2231-2234.

35. Chua, L., Zaumseil, J., Chang, J., Ou, E., Ho, P., Sirringhaus, H. & Friend, R. General observation of n-type field-effect behaviour in organic semiconductors. *Nature.* 434, (2005) 194-199.

36. Yan, H., Chen, Z., Zheng, Y., Newman, C., Quinn, J., Dötz, F., Kastler, M. & Facchetti, A. A high-mobility electron-transporting polymer for printed transistors. *Nature.* 457, (2009) 679-686.

37. Caironi, M., Bird, M., Fazzi, D., Chen, Z., Di Pietro, R., Newman, C., Facchetti, A. & Sirringhaus, H. Very Low Degree of Energetic Disorder as the Origin of High Mobility in an n-channel Polymer Semiconductor. *Adv. Funct. Mater.* 21, (2011) 3371-3381.

38. Luzio, A., Criante, L., D'Innocenzo, V. & Caironi, M. Control of charge transport in a semiconducting copolymer by solvent-induced long-range order. *Sci. Rep.* 3, (2013) 3425.

39. Li, J., Du, J., Xu, J., Chan, H. & Yan, F. The influence of gate dielectrics on a high-mobility n-type conjugated polymer in organic thin-film transistors. *Appl. Phys. Lett.* 100, (2012) 033301.

40. D'Innocenzo, V., Luzio, A., Petrozza, A., Fazzi, D. & Caironi, M. Nature of Charge Carriers in a High Electron Mobility Naphthalenediimide Based Semiconducting Copolymer. *Adv. Funct. Mater.* 24, (2014) 5584-5593.

41. Veres, J., Ogier, S., Leeming, S., Cupertino, D. & Mohialdin Khaffaf, S. Low-k Insulators as the Choice of Dielectrics in Organic Field-Effect Transistors. *Adv. Funct. Mater.* 13, (2003) 199-204.

42. Cnf.cornell.edu,. CNF - Photolithography Resist Processes and Capabilities. (2015). at http://www.cnf.cornell.edu/cnf_process_photo_resists.html

43. Schuettfort, T., Huettner, S., Lilliu, S., Macdonald, J., Thomsen, L. & McNeill, C. Surface and Bulk Structural Characterization of a High-Mobility Electron-Transporting Polymer. *Macromolecules.* 44, (2011) 1530-1539.

44. Steyrleuthner, R., Schubert, M., Howard, I., Klaumünzer, B., Schilling, K., Chen, Z., Saalfrank, P., Laquai, F., Facchetti, A. & Neher, D. Aggregation in a High-Mobility n-Type

Low-Bandgap Copolymer with Implications on Semicrystalline Morphology. *J. Am. Chem. Soc.* 134, (2012) 18303-18317.

45. Tautz, R., Da Como, E., Limmer, T., Feldmann, J., Egelhaaf, H., von Hauff, E., Lemaur, V., Beljonne, D., Yilmaz, S., Dumsch, I., Allard, S. & Scherf, U. Structural correlations in the generation of polaron pairs in low-bandgap polymers for photovoltaics. *Nat. Commun.* 3, (2012) 970.

46. Spano, F. Modeling disorder in polymer aggregates: The optical spectroscopy of regioregular poly(3-hexylthiophene) thin films. *J. Chem. Phys.* 122, (2005) 234701.

47. Zhao, N., Noh, Y., Chang, J., Heeney, M., McCulloch, I. & Sirringhaus, H. Polaron Localization at Interfaces in High-Mobility Microcrystalline Conjugated Polymers. *Adv. Mater.* 21, (2009) 3759-3763.

APPENDIX A

The modulation of the gate voltage applied over time also modulates charges on the gate electrode. The upper bound for modulation frequency is determined by the switching frequency of the OFETs in the order of $f_0 = \mu V_{GS,eff}/2\pi L^2 \approx 40kHz$, where μ is the carrier mobility, $V_{GS,eff}$ is the effective gate voltage where pinch-off of the charge carriers at the drain occurs and $V_{GS,eff} = V_{DS}$.[1] The modulation frequency used in CMS measurements were varied to investigate and affirm the choice of modulation frequency f = 170Hz used previously in ONDL lab.

The CMS spectra in Figure A.1 are single spectrum taken at different modulation frequency, at 0.05eV intervals, over a restricted energy range of 1.1eV to 2.0eV consisting of most prominent absorption feature at 1.49eV. The P(NDI2OD-T2) device used is with PS as gate dielectric.
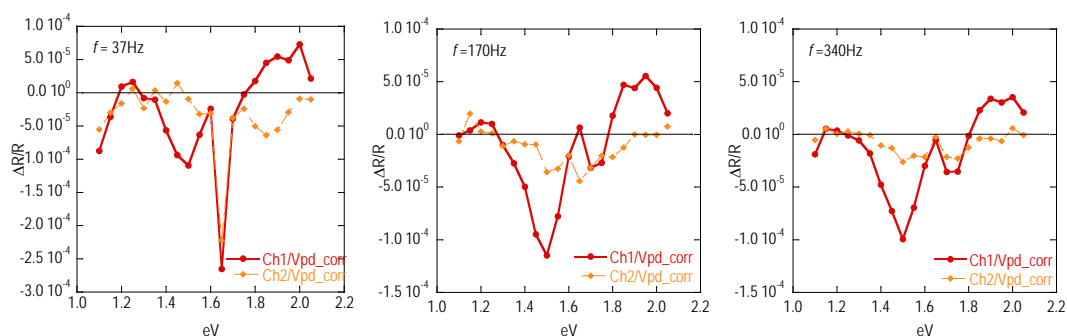

Figure A.1: CMS spectra of P(NDI2OD-T2)/PS device at modulation frequencies (a) f = 37Hz, (b) f = 170Hz, (c) f = 340Hz

The X (Ch1) and Y (Ch2) components of the CMS spectra were phase corrected as best as possible, but the quadrature signals for the lowest modulation frequency of 37Hz are still very significant. A non-zero quadrature indicates that reflection signals from slow and secondary processes in response to the modulating gate voltage are captured, which is not ideal. The quadrature signals decrease as increasing modulation frequency is used. However, at the highest frequency of 340Hz, the in-phase signal is smaller compared to that of 170Hz, such that some spectral features are dampened. Hence, a modulation frequency of 170Hz is used in the CMS study.

---

[1] Paasch, G., & Scheinert, S. (2004). Scaling organic transistors: materials and design. *Mater. Sci.-Poland*, *22* (4) 423-434.

Next, the effect of varying drain voltage was investigated, keeping in mind that reported CMS studies on P(NDI2OD-T2) devices are measured while varying gate voltage in the absence of a source-drain voltage. Figure A 2 below compares CMS measurements conducted at V_d = 15V and V_d = 0V for both frequencies of f = 170Hz and f = 340Hz. Similar to the above, the data was obtained at 0.05eV intervals, from 1.1eV to 2.0eV.

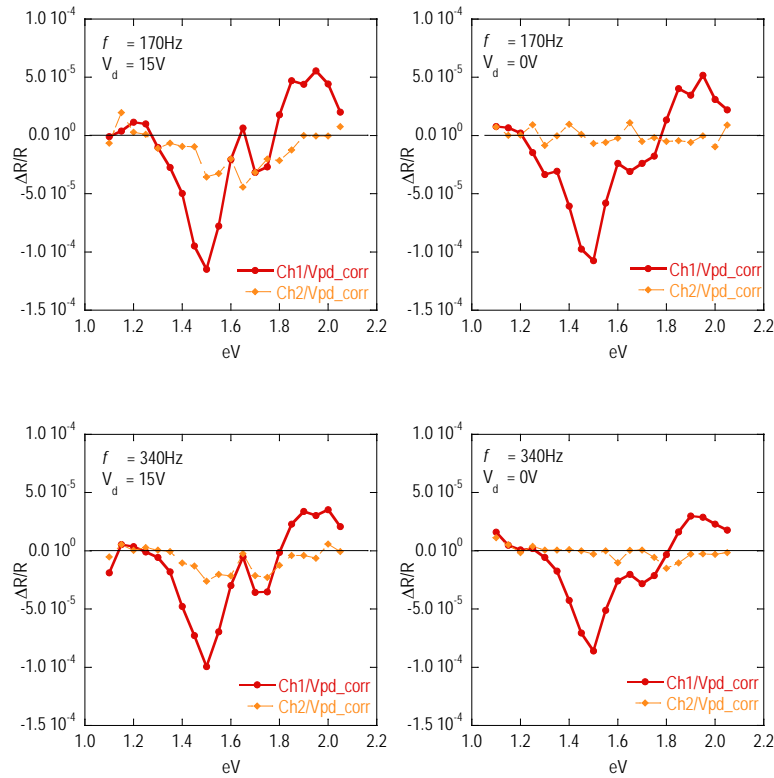*Figure A 2: CMS spectra of P(NDI2OD-T2)/PS device with Vg=50V, ΔVg=±10V, and Vd=15V (left) or Vd=0V (right) for (a) f = 170Hz, and (b) f = 340Hz*

For CMS spectra obtained at both frequencies, applying a drain voltage V_d = 15V gave more pronounced spectral features of two distinct absorption peaks. At V_d = 0V, the absorption peaks seemed to have merged into a broader peak with a small observable shoulder. Yet, the quadrature signals taken when zero source-drain voltage applied are easily phase corrected.

Since earlier literature has explored the spectra and their features when no source drain voltages were applied, the CMS study of P(NDI2OD-T2) devices in this report proceeded with the experimental condition of biasing a small source-drain voltage across the conduction channel. The condition allows the simulation of a normal operating device when probing the polaronic characteristics of the conducting polymer, and hopefully reveals new features in relation to existing findings.

APPENDIX B

Due to time constraints, only preliminary work was conducted to ascertain suitable OFETs to be used in mid-infrared (MIR) charge modulation spectroscopy (CMS). For CMS in the MIR range, a commercial Fourier Transform Infrared (FTIR) spectrometer was used in a step-scan experiment, modulating the applied gate voltage at each step-scan.[2] Instead of reflection mode used in optical and near-infrared CMS, MIR CMS operates in transmission mode.

Glass substrates used in this study for visible and near-infrared CMS are not transmitting in the mid-infrared (MIR) region, with percentage transmission (%T) falling to 0 for light with wavelength larger than 4000nm. Thus for the MIR CMS study, PET (polyethylene terephthalate) substrates were chosen due to their acceptable transmission ranges in the MIR region, and suitability in device fabrication.

Transmission tests were conducted to ensure that the dielectric and P(NDI2OD-T2) layers do not significantly block off any wavelength range within the MIR region. From Figure B.1, there is no drastic influence of the polymer films on transmission in the MIR range; each spectrum is similar to that obtained on blank PET substrate.
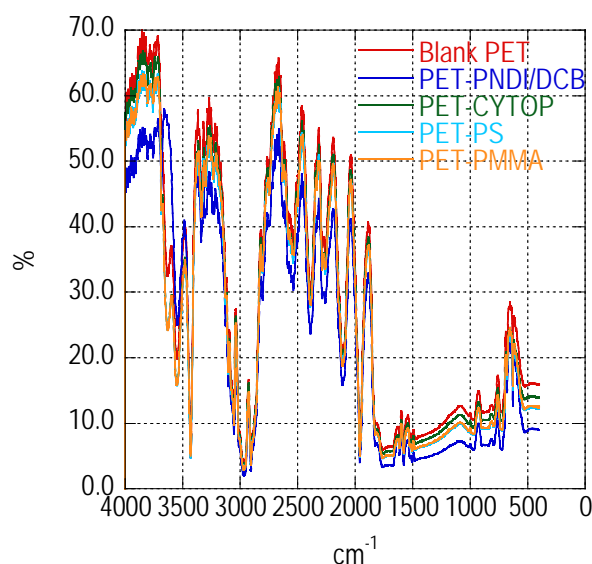

Figure B.1: MIR region transmission spectra of semiconductor or gate dielectric films on PET substrates compared with transmission of blank PET substrate

---

[2] JINGMEI, Z. (2011). *Morphology and Charge Transport in Polymer Organic Semiconductor Field-Effect Transistors* (Doctoral dissertation).

In addition, the thickness of a thin metal chromium-silver (Cr-Ag) gate electrode layer was calibrated for the devices to optimize signal transmission. Figure B.2 shows the variation of thickness of gate electrode with percentage transmission of the signal.
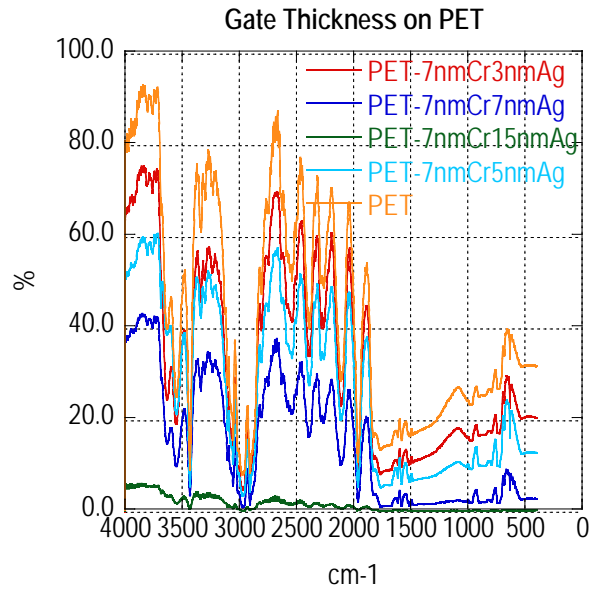

Figure B.2: MIR region transmission spectra of gate electrode layers of varying thickness compared with transmission of blank PET substrate

At the same time, good conductivity across the gate electrode has to be achieved for the measured gate voltage to be an accurate reflection of the actual voltage difference across the device region at the gate and source electrodes. It was found that a gate electrode of 7nm Cr and 3nm Ag is able to adhere on the polymer surface for CYTOP and PS, limited only by a small resistivity value. A slightly thicker gate electrode of 7nm Cr and 5nm Ag was found to give an acceptable resistivity value on the rougher surface of PMMA dielectric layer.